Seismic velocities from borehole measurements at four locations along a fifty-kilometer section of the San Andreas fault near Parkfield, California

by

James F. Gibbs[1], Edward F. Roth[2], Thomas E. Fumal[1]
Noreen A. Jasek[3] and Mark A. Emslie[3]

U.S. Geological Survey Open-File Report 90-248

---

[1]U.S. Geological Survey, MS 977, Menlo Park, CA 94025
[2]Deceased
[3]*National Association of Geology Teachers*, summer program

CONTENTS

ILLUSTRATIONS

ILLUSTRATIONS (Continued)

TABLES

INTRODUCTION

Shear-(S-waves) and compressional-waves (P-waves) were measured in boreholes at four locations along a section of the San Andreas fault near the hamlet of Parkfield in central California. This section of the San Andreas fault has a history of producing a magnitude 6+ earthquake approximately every 22 years. The predicted date for the next magitude 6+ earthquake is 1988 ± 5.2 years at the 95 percent confidence level (Bakun and Lindh, 1985). Because the region surrounding Parkfield is mostly range land it is an ideal location for field experiments. As a result a variety of seismic instrumentation has been deployed in anticipation of the magnitude 6+ earthquake. In fact, the boreholes in which we made P- and S-wave measurements were drilled and cased for the installation of downhole dilatometers (Myren and Johnston, 1989). Seismic wave velocities determined from these measurements are important parameters for estimating the seismic response of the near-surface geologic units. Because very little is known about near-fault ground response, these data will provide important velocity and attenuation information to supplement the interpretation of anticipated recordings of strong ground motions. Of the four boreholes logged for seismic velocities (from northwest to southeast, Stockdale Mountain, Vineyard Canyon, Jack Canyon, and Red Hills) only Jack Canyon is on the northeast side of the San Andreas fault (Figure 1). Differences in seismic velocity are due for the most part, to the changes in lithology that are observed on opposite sides of the San Andreas fault. A detailed analysis of velocity and attenuation was made using data from Vineyard Canyon site (Gibbs and Roth, 1989). Shear-wave anisotropy of approximately 20 percent and a low shear-wave Q of 4 were determined from velocity measurements at Vineyard Canyon. Attenuation studies using data from Stockdale Mountain, Red Hills, and Jack Canyon have not been completed.

GEOLOGIC SETTING

The topography of the region surrounding the segment of the San Andreas fault shown in Figure 1, consists of the Cholame Hills and the Temblor Range on the southwest side of the fault and the southern end of the Diablo Range that includes Middle Mountain, Table Mountain, and Avenal Ridge on the northeast side.

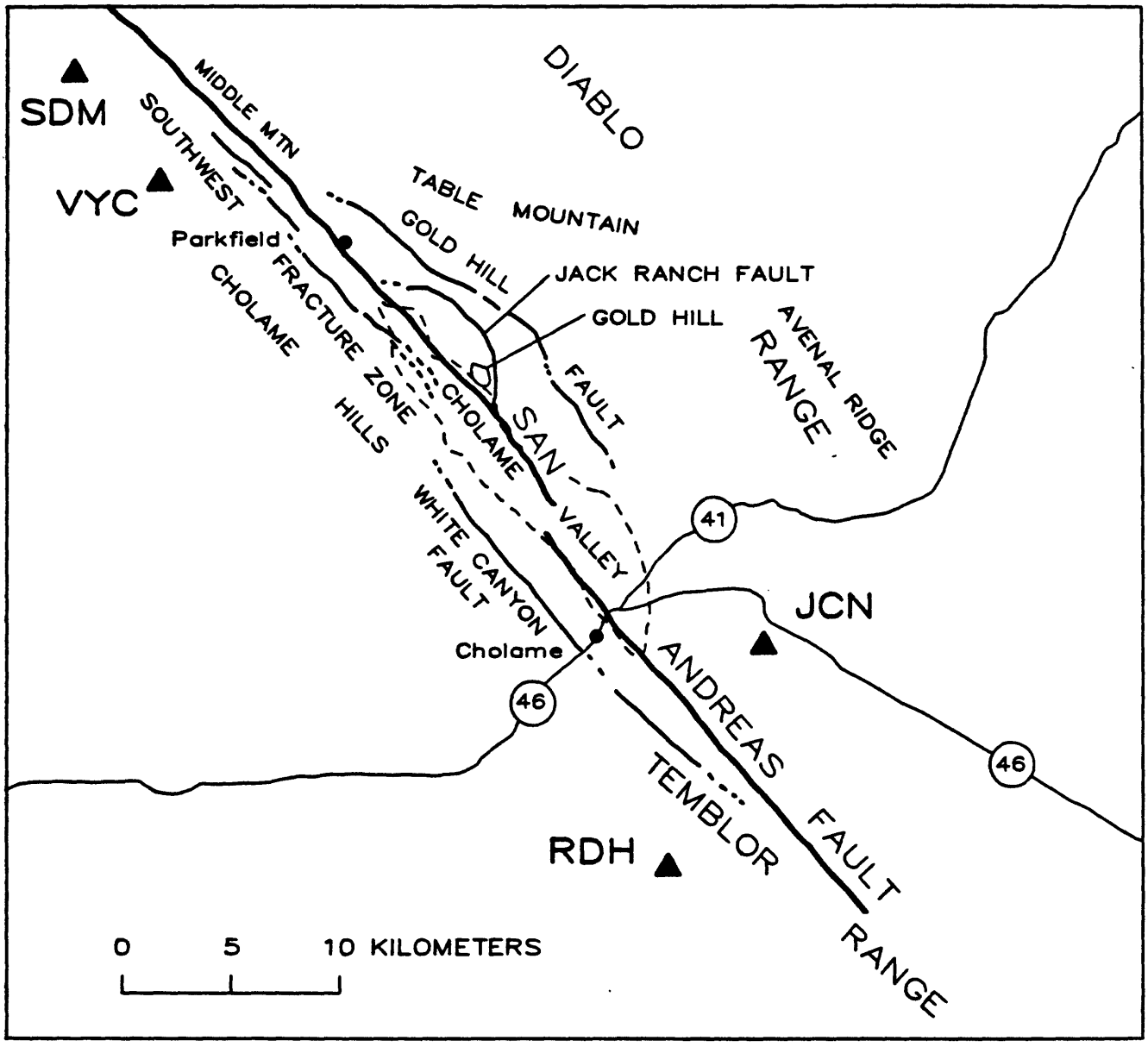

Figure 1. Map showing the region surrounding the segment of the San Andreas fault near Parkfield, California. Borehole locations are shown by triangles. Tectonics after Sims and Hamilton, (in press).

The change in elevation from the floor of Cholame Valley to the surrounding peaks is approximately 600 meters.

The tectonics of the area are extremely complex. Major features (Sims, 1988) of this segment include:

1. Offset of the San Andreas fault under the Cholame Valley.
2. Gold Hill and Jack Ranch thrust faults on the northeast side of the San Andreas fault.
3. Southwest Fracture Zone and White Canyon fault parallel the San Andreas fault on the southwest side (Figure 1).
4. The allochthonous Gold Hill block has been offset 315 km from the San Emigdio mountains by movement along the San Andreas fault (Ross, 1970; Sims, 1988).
5. Rocks to the northeast side of the San Andreas fault generally are older consisting of Jurassic and Cretaceous strata and Miocene sedimentary units.
6. Southwest of the San Andreas fault the oldest rocks exposed are early Miocene.

BOREHOLE MEASUREMENTS

The field procedures used to obtain the borehole data have been described by Warrick, 1974, Gibbs et al.,1975, and Gibbs and Roth, 1988. Only a brief description of field techniques is given here. A three-component geophone with one vertical and two orthogonal horizontal sensors is lowered into the borehole and clamped into position. Measurements of P- and S-waves are made at depth intervals along the axis of the borehole $2\frac{1}{2}$ or 5 meters depending on thickness of strata. The $2\frac{1}{2}$-meter spacing is used for thinly bedded (< 15 *meters*) strata. In thickly bedded strata (> 15 *meters*) the 5-meter spacing is used. Shear-waves are generated by striking opposite ends of a plank held in place by the wheels of a truck. The hammer blows produce a reversible shear-wave pulse. The method is essentially that described by Warrick, 1974, as the *horizontal traction method* for shear-waves and was first applied in Japan by Kobayashi, 1959. However, the introduction of a new shear-wave source (Liu, et al., 1988) has streamlined procedures by eliminating a hand actuated hammer for a more consistent horizontal blow. The new shear-source is powered by compressed air and provides a consistent repeatable pulse for stacking data and for attenuation studies. This new source was used throughout this study.

Compressional waves (P-waves) were generated by striking a steel plate with a sledge hammer. The data were recorded on cassette tapes at 1028 samples per second with a twelve-channel digital recorder.

INTERPRETATION OF BOREHOLE DATA

To aid in identifing the onset of the S-wave, we make use of the fact that the polarity of the shear-wave can be reversed by changing the direction of the horizontal pulse. This is accomplished with the air-powered shear generator by alternately driving the hammer against a stop located at each end of the generator. The signals recorded from impacts in opposite directions are superimposed and plotted on a common time base. The zero-crossing can be readily identified by this method and is used as the primary S-wave arrival time; in addition, a peak or trough is timed to provide a velocity check. These data are plotted on a time-depth graph, Figures 2– 6, and fit with straight lines by the method of least squares. Depth intervals for determination of velocities are based on changes in lithology and changes in the slope of the line fit to the data points. Primary consideration is given to changes in slope and geologic materials since subtle changes in lithology often do not cause changes in velocity. Studies in the San Francisco bay region (Fumal, 1978) have found that changes in shear-wave velocity correlate best with various sets of physical properties. For unconsolidated to semiconsolidated sedimentary units, texture (relative grain size distribution) was found to have the most significant effect on shear-wave velocity. For bedrock materials fracture spacing was found to have the most significant effect on shear-wave velocity. Hardness has the second largest effect, and lithology may account for velocity differences between hard-sedimentary and igneous rocks.

SEISMIC VELOCITIES

Two methods of calculating shear-wave velocities are used for the data in this report. ***Interval velocities*** shown in Tables 1– 4, are calculated from the inverse slope of the straight-line segments shown on the time-depth graphs Figures 5, 7, 9, 11 and 12. The uncertainty interval of these velocities is calculated from the high and low estimates of the slope, (RLONE, 1981). We interpret this to mean that the true value lies in the uncertainty interval and the statement can be made with 95 percent confidence.

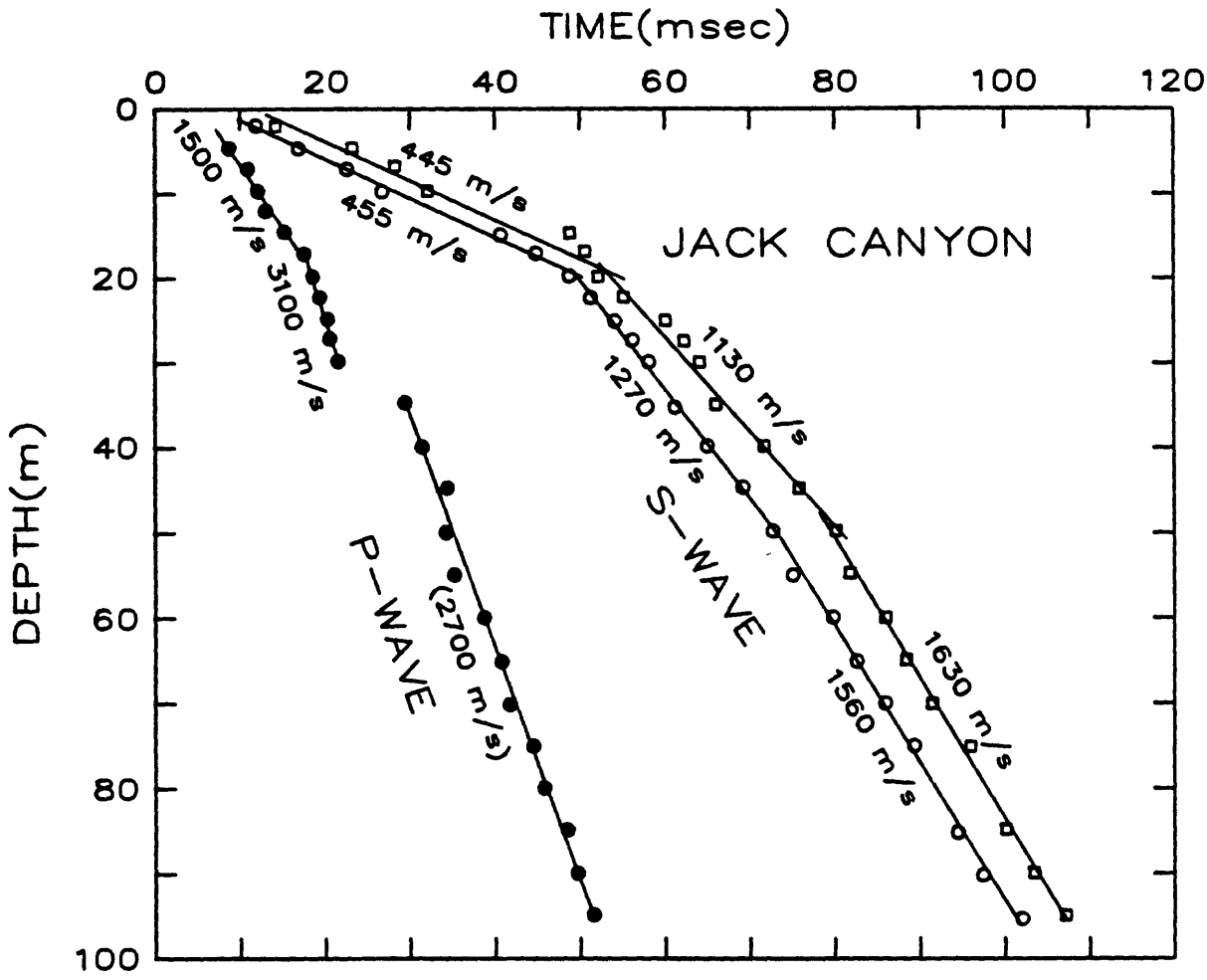

Figure 2. Time-depth graph for Jack Canyon with velocities shown near line segments. Open circles and squares are S-wave picks, solid circles are P-wave picks. Velocities are determined from the reciprocal of the slope of the line segments and uncertainty intervals are calculated at the 95 percent confidence level, Table 1.

TABLE 1

INTERVAL VELOCITIES: JACK CANYON BOREHOLE

		S-WAVE ZERO-CROSSING		SECOND S-PICK	
DEPTH INTERVAL (M)	NUMBER POINTS	INTERVAL VELOCITY (M/S)	UNCERTAINTY INTERVAL (M/S)	INTERVAL VELOCITY (M/S)	UNCERTAINTY INTERVAL (M/S)
2.5—20.0	7	454	(420—495)	444	(366—565)
20.0—50.0	9	1275	(1205—1351)	1125	(1000—1282)
50.0—95.0	9	1563	(1471—1667)	1633	(1538—1754)

	P-WAVE FIRST ARRIVAL		
DEPTH INTERVAL (M)	NUMBER POINTS	INTERVAL VELOCITY (M/S)	UNCERTAINTY INTERVAL (M/S)
5.0—17.5	6	1472	(1299—1695)
17.5—30.0	6	3098	(2439—4167)
35.0—95.0	13	2701	(2564—2857)

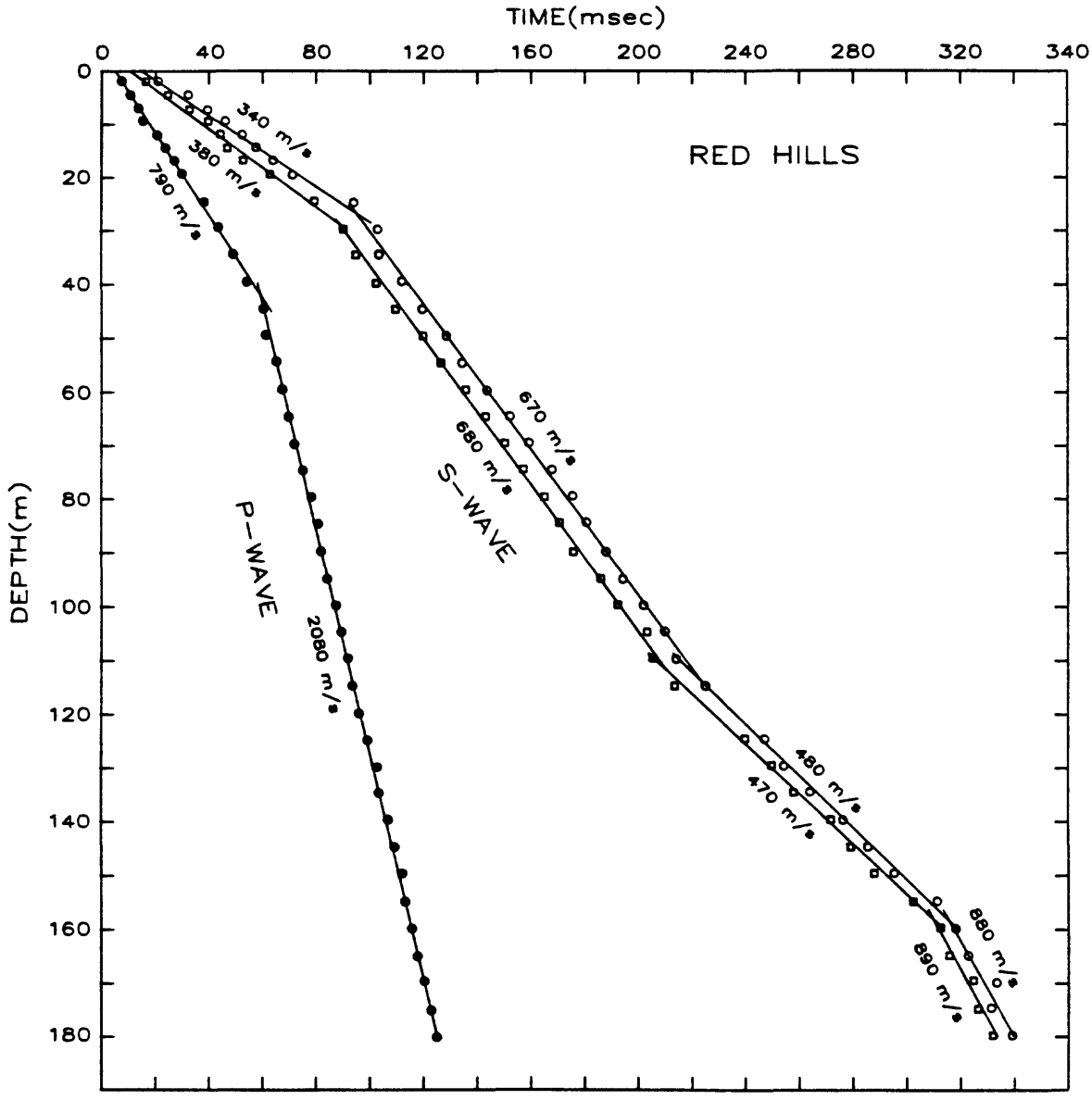

Figure 3. Time-depth graph for Red Hills with velocities shown near line segments. Open circles and squares are S-wave picks, solid circles are P-wave picks. Velocities are determined from the reciprocal of the slope of the line segments and uncertainty intervals are calculated at the 95 percent confidence level, Table 2.

TABLE 2

INTERVAL VELOCITIES: RED HILLS BOREHOLE

		S-WAVE ZERO-CROSSING		SECOND S-PICK	
DEPTH INTERVAL (M)	NUMBER POINTS	INTERVAL VELOCITY (M/S)	UNCERTAINTY INTERVAL (M/S)	INTERVAL VELOCITY (M/S)	UNCERTAINTY INTERVAL (M/S)
2.5—30.0	10	381	(352—415)	341	(313—373)
30.0—115.0	18	677	(662—694)	675	(658—690)
115.0—155.0	8	467	(433—508)	482	(450—518)
155.0—180.0	6	888	(690—1235)	883	(662—1316)

	P-WAVE FIRST ARRIVAL		
DEPTH INTERVAL (M)	NUMBER POINTS	INTERVAL VELOCITY (M/S)	UNCERTAINTY INTERVAL (M/S)
2.5—45.0	13	789	(763—820)
45.0—180.0	28	2080	(2041—2128)

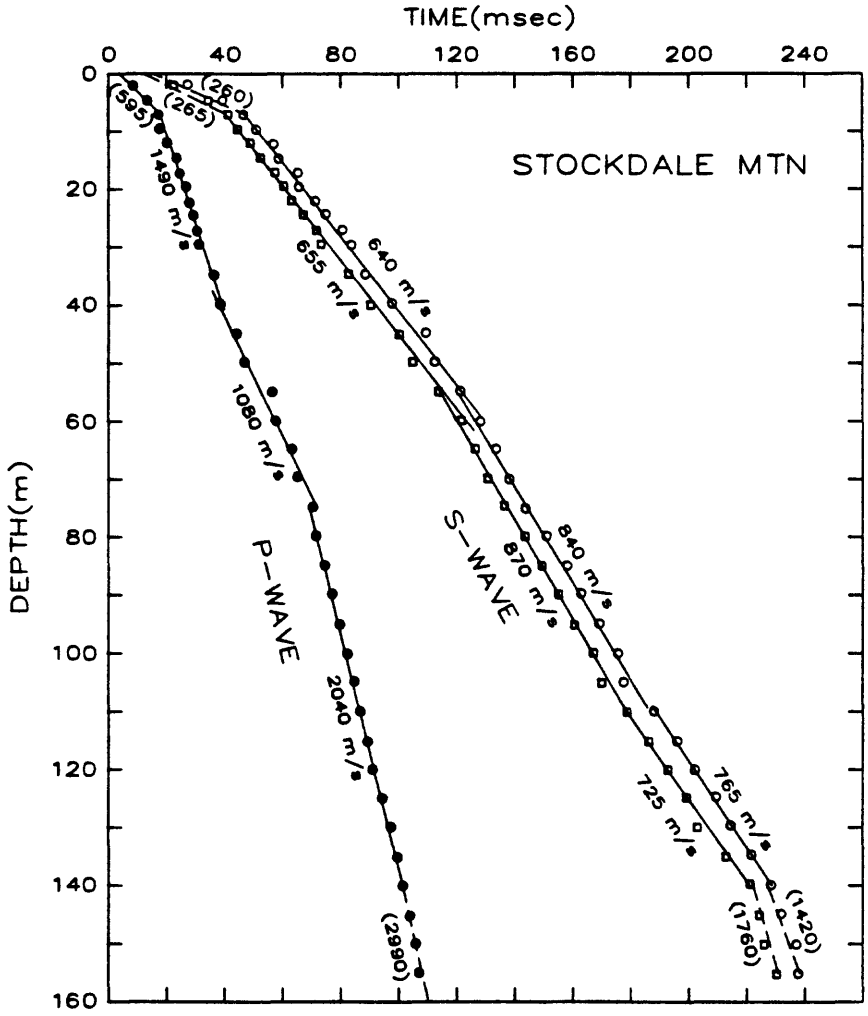

Figure 4. Time-depth graph for Stockdale Mountain with velocities shown near line segments. Open circles and squares are S-wave picks, solid circles are P-wave picks. Velocities are determined from the reciprocal of the slope of the line segments and uncertainty intervals are calculated at the 95 percent confidence level, Table 3.

TABLE 3

INTERVAL VELOCITIES: STOCKDALE MOUNTAIN BOREHOLE

DEPTH INTERVAL (M)	NUMBER POINTS	S-WAVE ZERO-CROSSING INTERVAL VELOCITY (M/S)	S-WAVE ZERO-CROSSING UNCERTAINTY INTERVAL (M/S)	SECOND S-PICK INTERVAL VELOCITY (M/S)	SECOND S-PICK UNCERTAINTY INTERVAL (M/S)
2.5—7.5	3	[1](264)	—	(262)	—
7.5—60.0	16	655	(641—671)	642	(621—667)
60.0—110.0	11	871	(840—901)	839	(794—885)
110.0—140.0	7	724	(649—820)	764	(741—787)
140.0—155.0	4	(1758)	(1266—2857)	(1419)	(806—5882)

DEPTH INTERVAL (M)	NUMBER POINTS	P-WAVE FIRST ARRIVAL INTERVAL VELOCITY (M/S)	P-WAVE FIRST ARRIVAL UNCERTAINTY INTERVAL (M/S)
2.5—7.5	3	(595)	—
7.5—40.0	12	1489	(1389—1613)
40.0—75.0	8	1082	(943—1266)
75.0—140.0	14	2038	(1961—2083)
140.0—155.0	4	(2990)	(2128—5263)

[1]Interval velocities enclosed in parenthesis are determined from 4 or fewer points and generally have large uncertainty intervals.

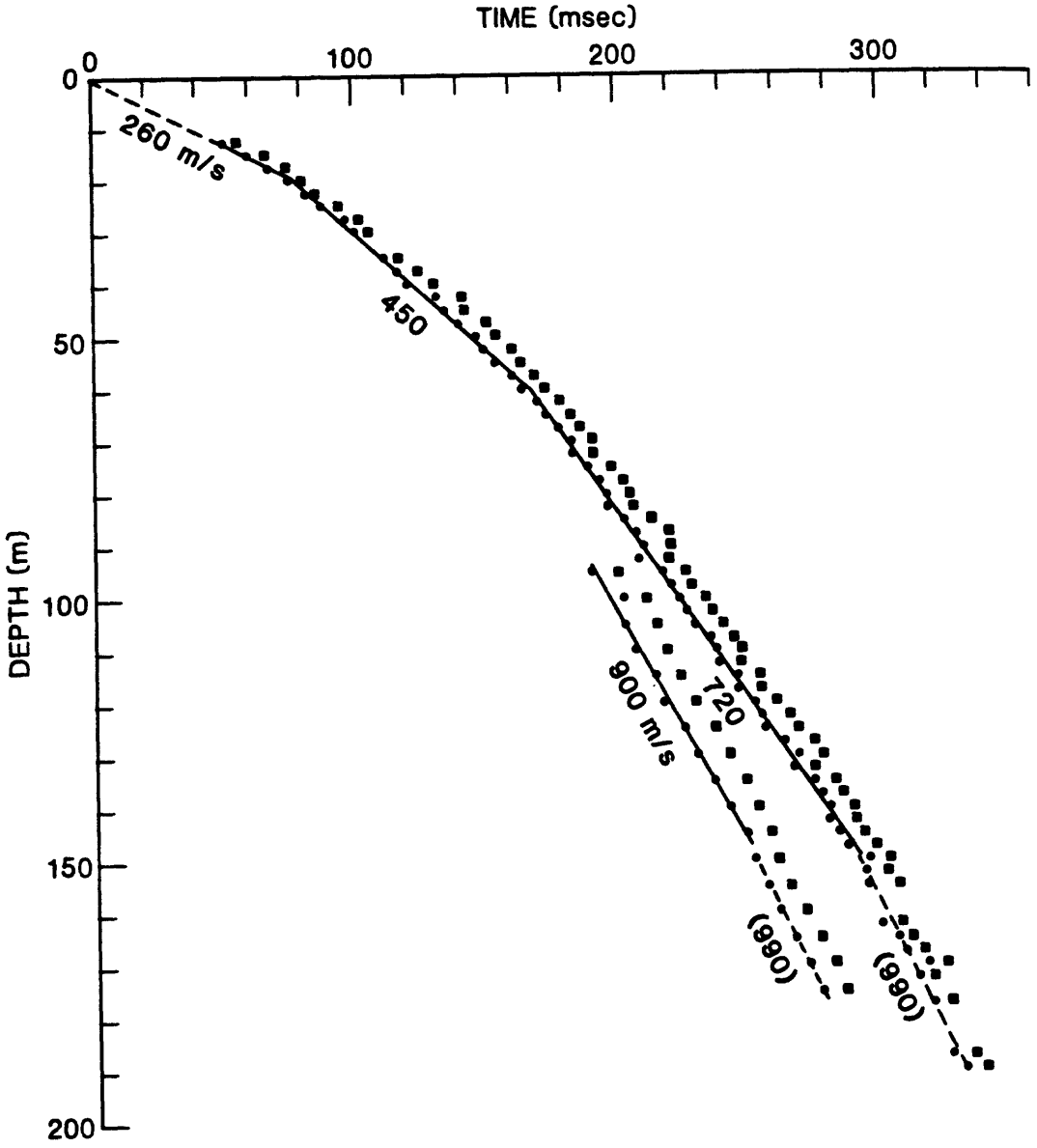

Figure 5. Time-depth graph for Vineyard Canyon showing S-wave velocities calculated from the reciprocal of the slope of the line segments. The 900 m/s velocity was determined from a 90 degree change in the direction of the horizontal source indicating material anisotropy of approximately 20 percent.

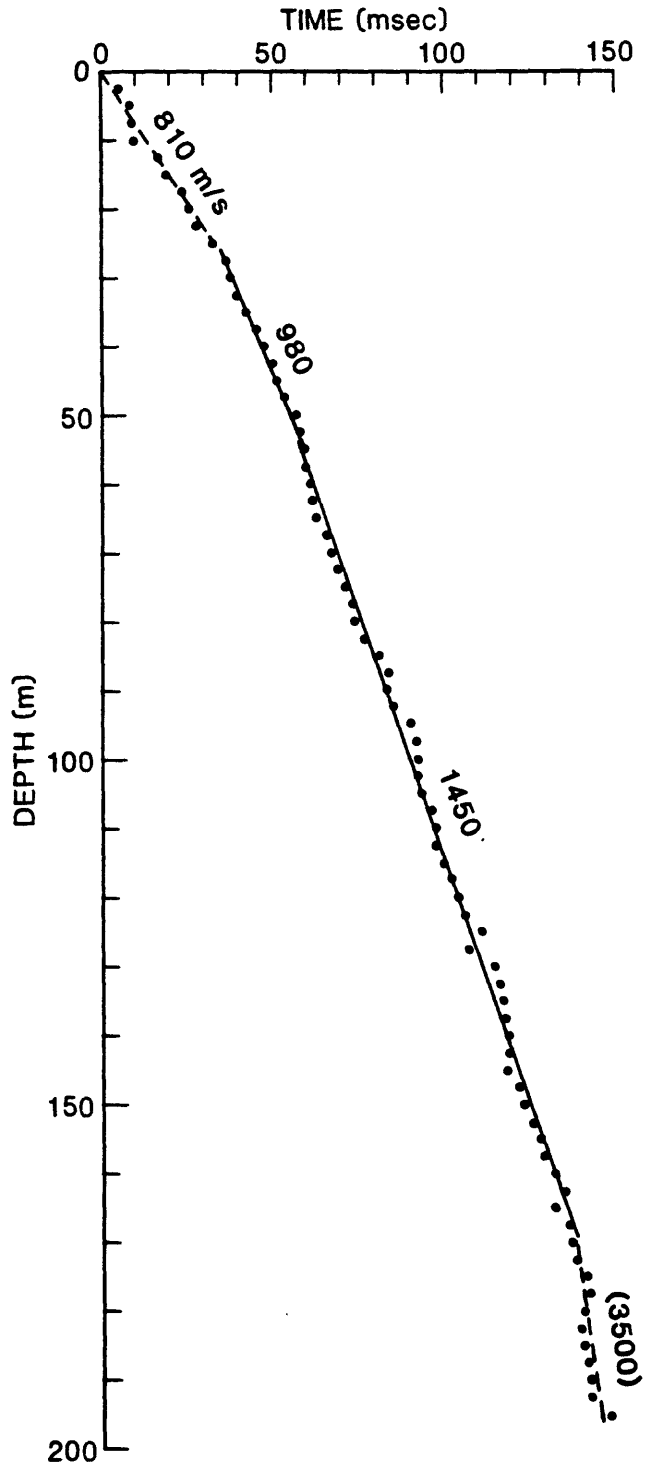

Figure 6. Time-depth graph for Vineyard Canyon showing P-wave velocities calculated from the reciprocal of the slope of the line segments. Velocity uncertainty intervals are shown in Table 4.

TABLE 4

INTERVAL VELOCITIES: VINEYARD CANYON BOREHOLE

		S-WAVE ZERO-CROSSING		SECOND S-PICK	
DEPTH INTERVAL (M)	NUMBER POINTS	INTERVAL VELOCITY (M/S)	UNCERTAINTY INTERVAL (M/S)	INTERVAL VELOCITY (M/S)	UNCERTAINTY INTERVAL (M/S)
0.0—20.0	4	[1](256)	(243—271)	(234)	(217—254)
20.0—60.0	17	453	(437—470)	426	(409—445)
60.0—155.0	39	724	(712—737)	720	(707—733)
162.5—190.0	8	992	(770—1395)	922	(746—1208)

	P-WAVE FIRST ARRIVAL		
DEPTH INTERVAL (M)	NUMBER POINTS	INTERVAL VELOCITY (M/S)	UNCERTAINTY INTERVAL (M/S)
0.0—25.0	10	813	(741—901)
25.0—55.0	13	984	(909—1075)
55.0—170.0	44	1448	(1408—1493)
170.0—195.0	11	3493	(2222—8333)

[1]Interval velocities enclosed in parenthesis are determined from 4 or fewer points and generally have large uncertainty intervals.

Following Draper and Smith (1966) the estimated standard error (*s.e.*) of the slope is:

$$s.e.(b_1) = \frac{s}{\{\sum(X_i - \bar{X})^2\}^{\frac{1}{2}}}$$

where

$$s = \sqrt{\frac{ss}{n-2}}$$

and ss is the sum of the squares of the residuals, n is the sample size, and $(n-2)$ the number of degrees of freedom. Estimated limits for the slope (b_1) are:

$$b_1 \pm \frac{t(n-2, 1-\frac{1}{2}\alpha)s}{\{\sum(X_i - \bar{X})^2\}^{\frac{1}{2}}}$$

where t is the test for significance from the t-table and $(n-2, 1-\frac{1}{2}\alpha)$ is the $(1-\frac{1}{2}\alpha)$ percentage point of a t-distribution with $(n-2)$ degrees of freedom, and percentage confidence limits are equal to $100(1-\alpha)$. In our case α is equal to 0.05 at the 95 percent confidence level.

A summary of the interval velocities is shown in Figures 7 and 8. The shear-wave velocities at Red Hills, Vineyard Canyon, and Stockdale Mountain are very similar. These borehole locations are on the southwest side of the San Andreas fault. Jack Canyon on the northeast side of the fault has a significantly higher shear-wave velocity at depths below 20 meters. Similarily, P-wave velocities at Jack Canyon are higher than those on the southwest side of the San Andreas fault at depths below 20 meters.

The ***average velocity*** shown in Tables 5– 8, is the depth divided by the corrected arrival time ($cos\phi$ times the observed slant time).

ACKNOWLEDGEMENTS

We thank our colleagues Ron Porcella, Robert Westerlund for their field work assistance, Malcolm Johnston for making the finished boreholes available for velocity measurements; John Sims and Dave Higgins for providing geologic logs from unpublished data. We are saddened by the death of our colleague Edward Roth after a heart operation on October 20, 1988.

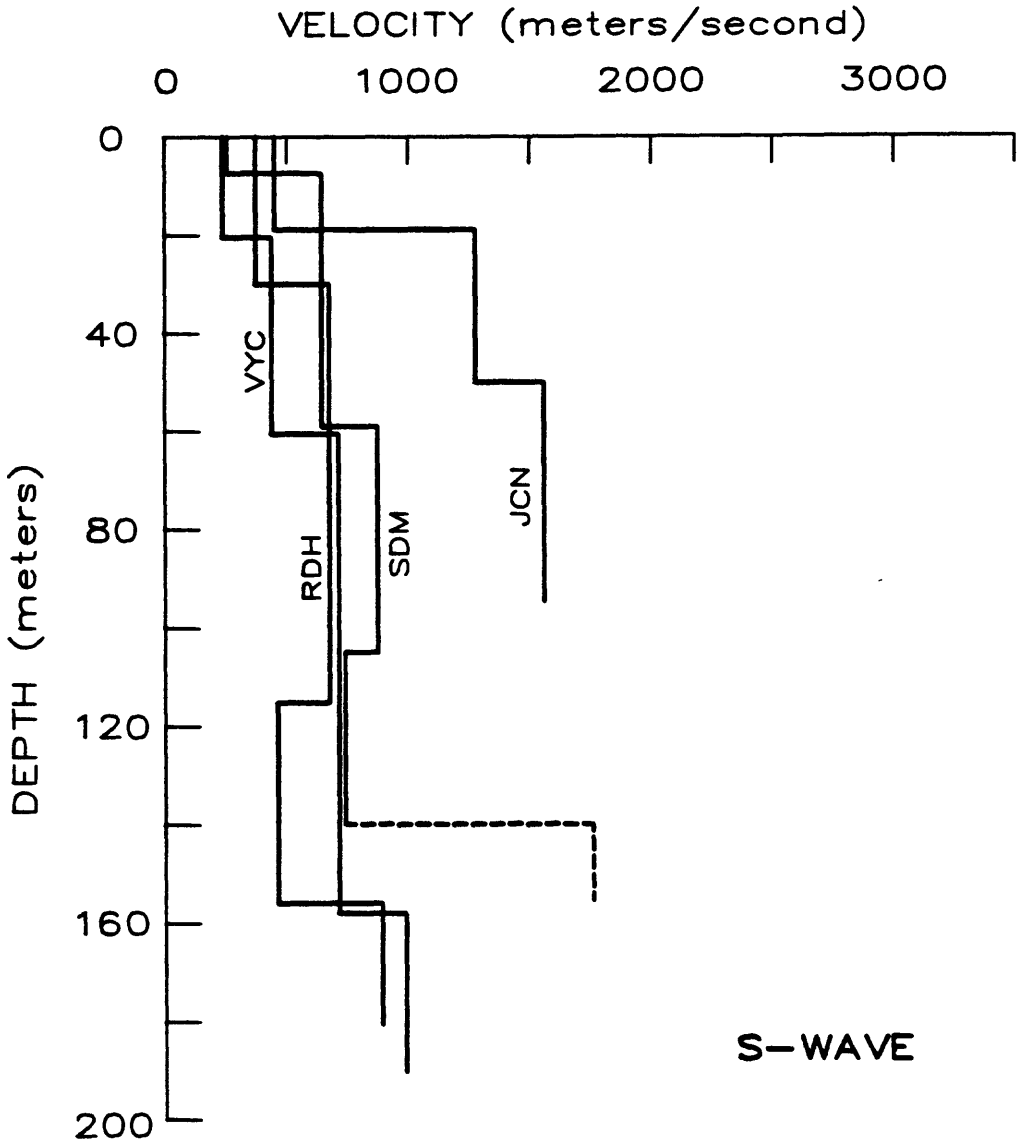

Figure 7. S-wave velocity summaries at Jack Canyon (JCN), Red Hills (RDH), Vineyard Canyon (VYC) and Stockdale Mountain (SDM). Dashed lines indicate greater uncertainty in velocity.

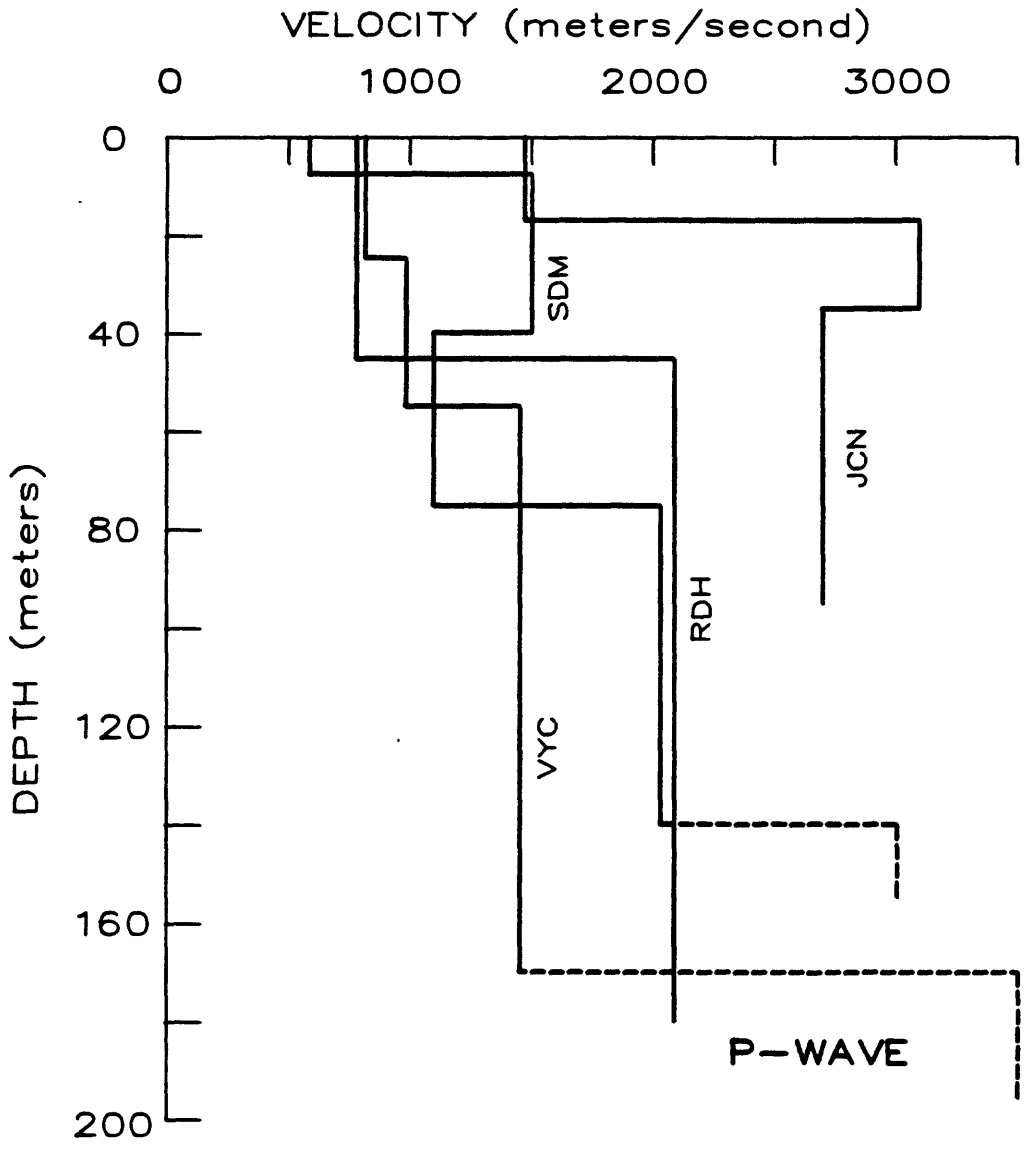

Figure 8. P-wave velocity summaries at Jack Canyon (JCN), Red Hills (RDH), Vineyard Canyon (VYC) and Stockdale Mountain (SDM). Dashed lines indicate greater uncertainty in velocities.

REFERENCES

Bakun, W. H. and Lindh, A.G., (1985), The Parkfield, California earthquake prediction experiment, *Science*, v. 229, p. 619-624.

Dibblee, T.W., Jr., (1974), Geologic map of the Shandon and Orchard Peak quadrangles, San Luis Obispo and Kern Counties, California, showing Mesozoic and Cenozoic rock units juxtaposed along the San Andreas fault: U.S. Geological Survey Miscellaneous Geologic Investigations Map I-788, scale 1:62,500.

Draper, N.R. and Smith, H., (1966), *Applied Regression Analysis*, p. 1-35, John Wiley and Sons, Inc., New York, New York.

Fumal, T.E., (1978), Correlations between seismic wave velocities and physical properties of near-surface geologic materials in the southern San Francisco Bay region, *U.S. Geological Survey Open-File Report 78-1067*, 114 p.

Gibbs, James F., Fumal, Thomas E., and Borcherdt, Roger D., (1975), In-situ measurements of seismic velocities at twelve locations in the San Francisco Bay region, *U.S. Geological Survey Open-File Report 75-564*.

Gibbs, James F. and Roth, Edward F., (1989), Seismic velocities and attenuation measurements near the Parkfield prediction zone, central California, *Earthquake Spectra*, v. 5, p. 513-537.

Kobayashi, N., (1959), A method of determining the underground structure by means of SH waves, *Zisin*, ser. 2, v. 12, p. 19-24.

Liu, Hsi-Ping, Warrick, Richard E., Westerlund, Robert E., Fletcher, Jon B., and Maxwell, Gary L., (1988), An airpowered impulsive shear-wave source with repeatable signals, *Bull. Seism. Soc. Am.*, v. 78, p. 355-369.

Myren, G.D. and Johnston, M.J.S., (1989), Borehole dilatometer installation, operation and maintenance at sites along the San Andreas fault, California, *U.S. Geological Survey, Open-File Report, 89-349*.

RLONE, (1981), IMSL library computer routine, Analysis of simple linear regression model, IMSL Inc., Houston, Texas.

Ross, D.C., (1970), Quartz gabbro and anorthositic gabbro: Makers of offset along the San Andreas fault in the California Coast Range, *Bull., Geol. Soc. Am.*, v. 81, p. 3647-3662.

Sims, John D., (1988), Geologic map of the San Andreas fault zone in the Cholame Valley and Cholame Hills quadrangles, San Luis Obisbo and Monterey Counties, California, U.S. Geological Survey, Map MF-1995.

Sims, J.D., and Hamilton, J.C., in press, Geologic map of Cholame Quadrangle, San Luis Obispo County, California: U.S. Geological Survey Miscellaneous Field Studies Map MF- , scale 1:24,000.

Warrick, R.E., (1974), Seismic investigations of a San Francisco Bay mud site, *Bull., Seism. Soc. Am.*, v. 64, p. 375-385.

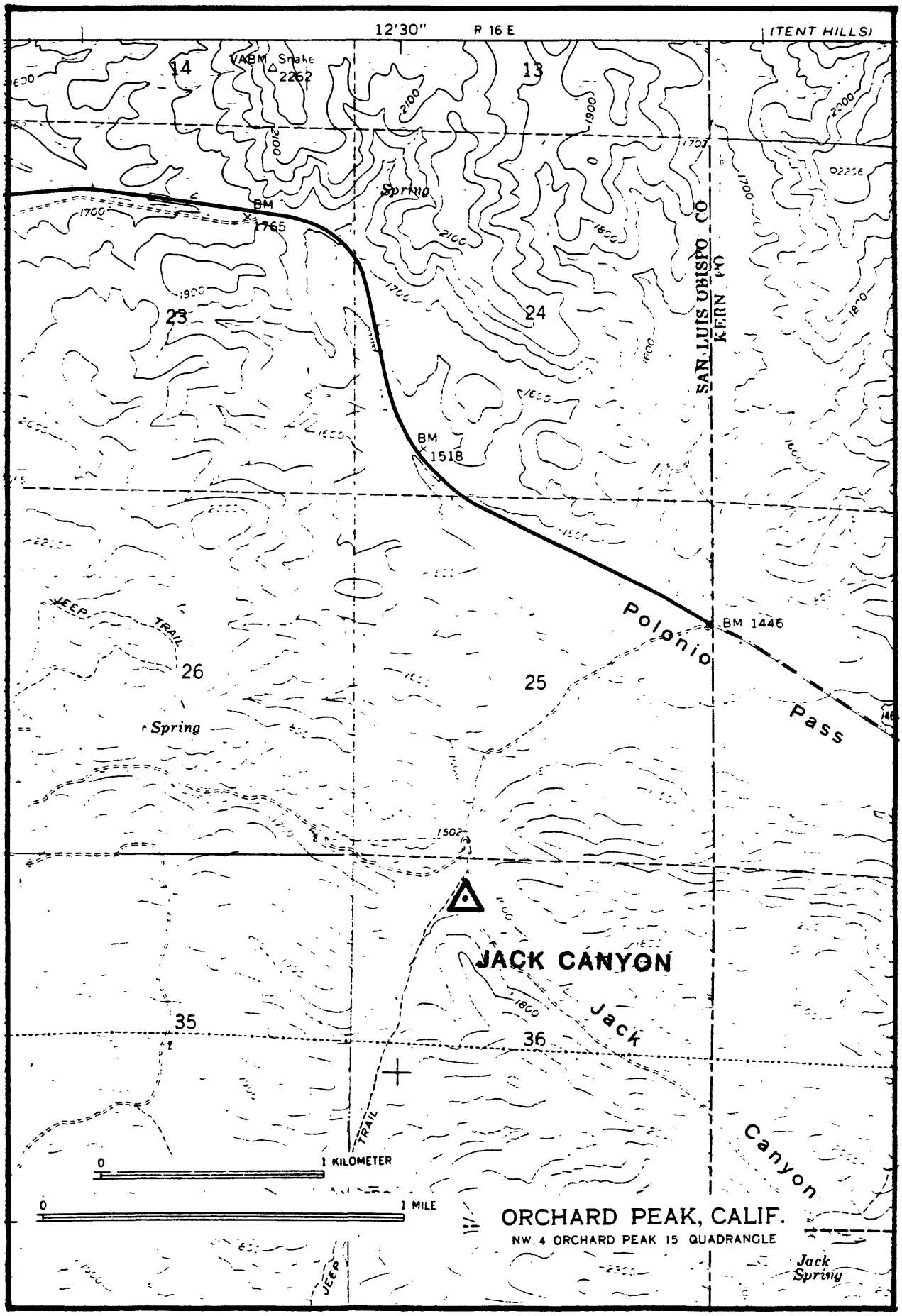

Figure 9. Location map of Jack Canyon borehole.

Site: JACK CANYON

Borehole completed: 5-27-86
Location: Lat. 35°42.9'N
Long. 120°12.3'W

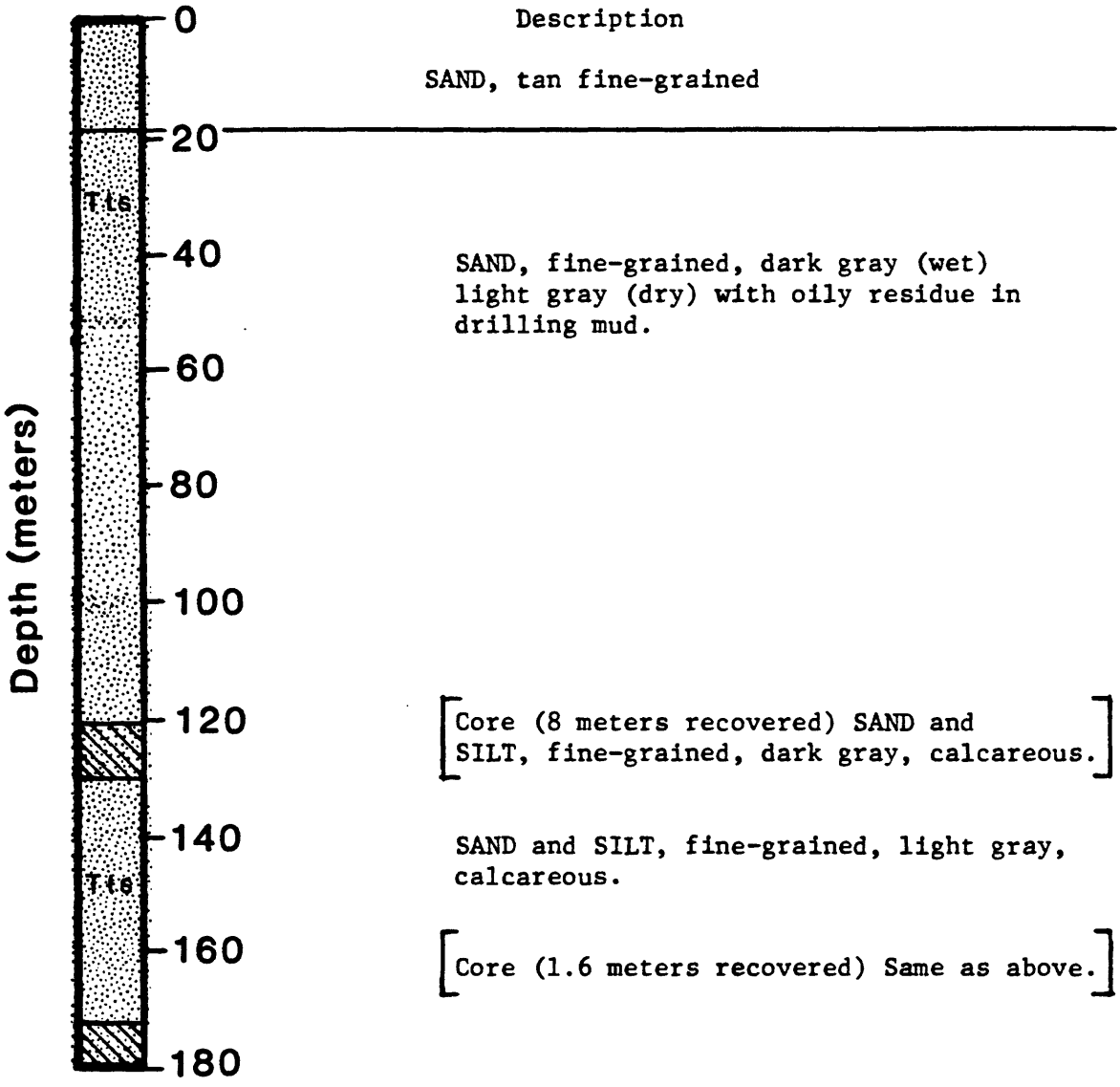

Figure 10. Geologic log of Jack Canyon borehole. Compiled from descriptions of drill cuttings and cores. Geologic map units are from Dibblee (1974).

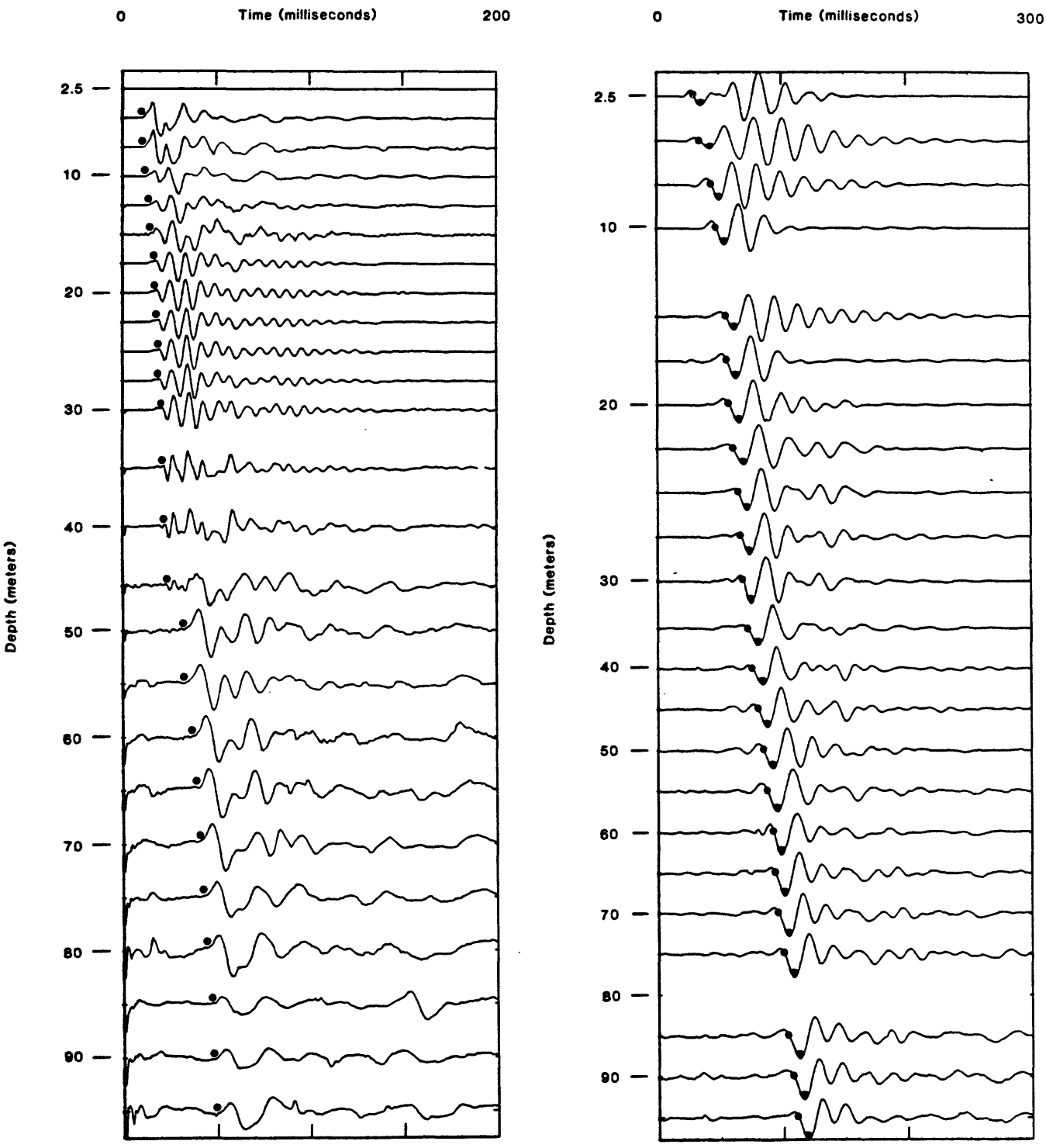

Figure 11. Jack Canyon record section showing P-wave (left) and S-wave picks. Two picks are shown for the S-wave: zero-crossings (dots) and troughs (filled).

TABLE 5

TRAVELTIMES AND AVERAGE VELOCITIES: JACK CANYON BOREHOLE

Site Abbreviation: JCN
Source Offset: S-Wave = 4.0 m

Date Logged: 1-15-87
P-Wave = 4.0 m

	S-WAVE		P-WAVE	
DEPTH (M)	ZERO-CROSSING (S)	AVE VEL (M/S)	FIRST BREAK (S)	AVE VEL (M/S)
2.5	0.011	219	—	—
5.0	0.017	299	0.008	598
7.5	0.022	336	0.010	726
10.0	0.026	381	0.012	848
12.5	—	—	0.013	965
15.0	0.040	370	0.015	995
17.5	0.045	392	0.017	1020
20.0	0.049	410	0.018	1102
22.5	0.051	442	0.019	1172
25.0	0.054	464	0.020	1235
27.5	0.056	492	0.020	1356
30.0	0.058	517	0.021	1408
35.0	0.061	574	0.029	1202
40.0	0.065	616	0.032	1248
45.0	0.069	653	0.034	1325
50.0	0.073	686	0.035	1429
55.0	0.075	734	0.035	1571
60.0	0.080	753	0.039	1542
65.0	0.083	786	0.041	1592
70.0	0.086	817	0.042	1673
75.0	0.090	837	0.045	1673
80.0	—	—	0.046	1749
85.0	0.094	900	0.049	1747
90.0	0.097	924	0.050	1813
95.0	0.102	928	0.052	1839

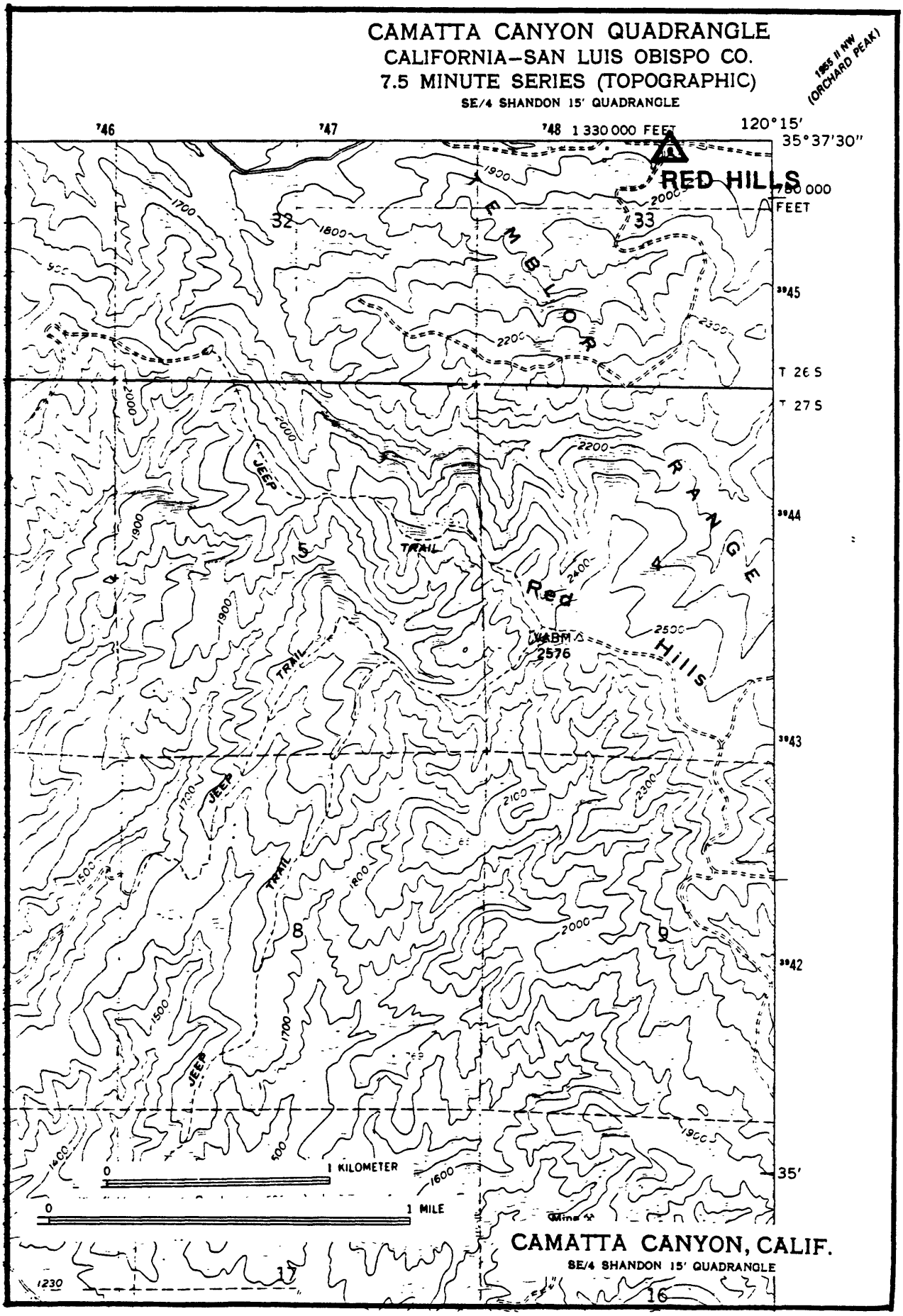

Figure 12. Location map of Red Hills borehole.

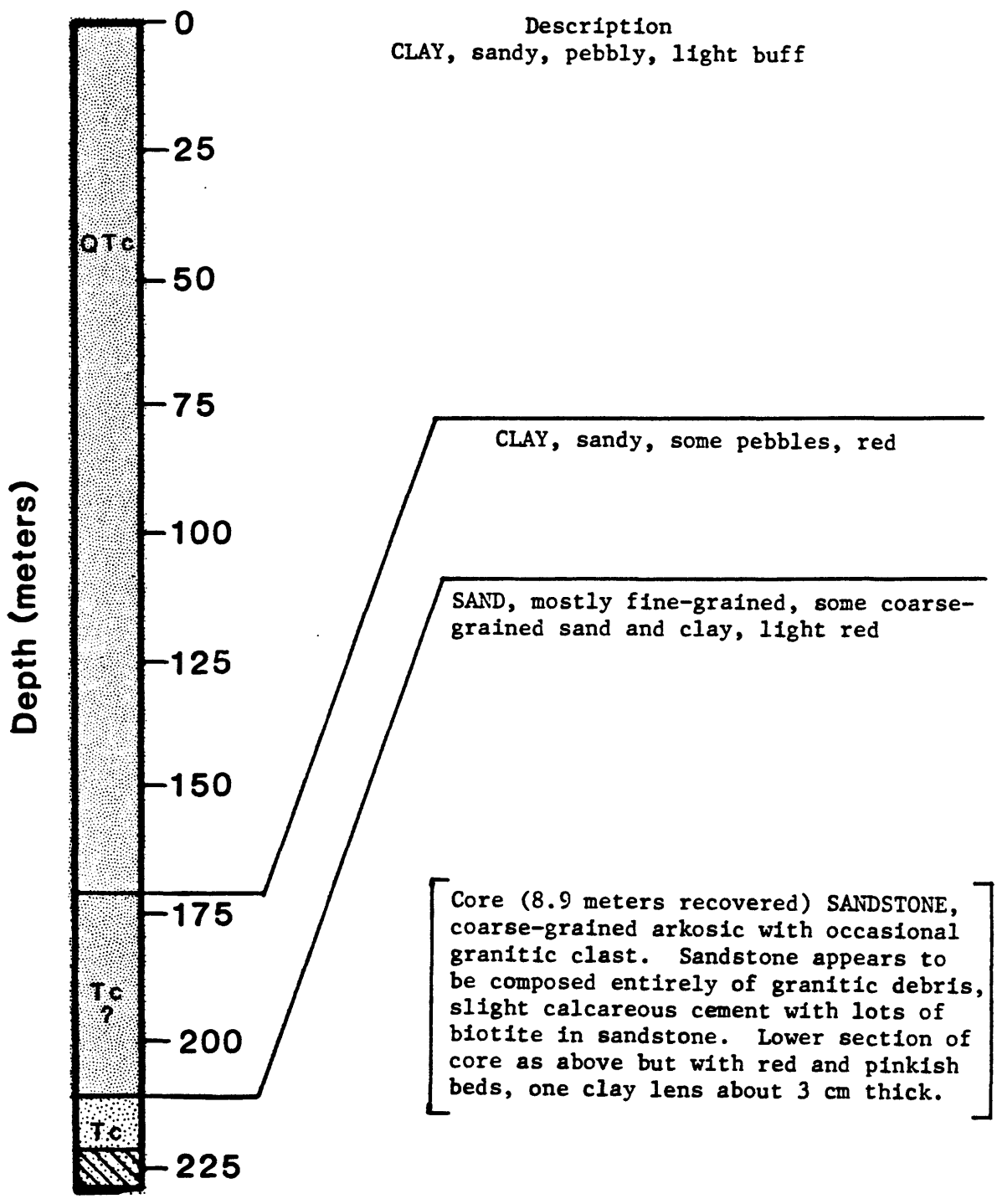

Figure 13. Geologic log of Red Hills borehole. Compiled from descriptions of drill cuttings and cores. Geologic map units are from Dibblee (1974).

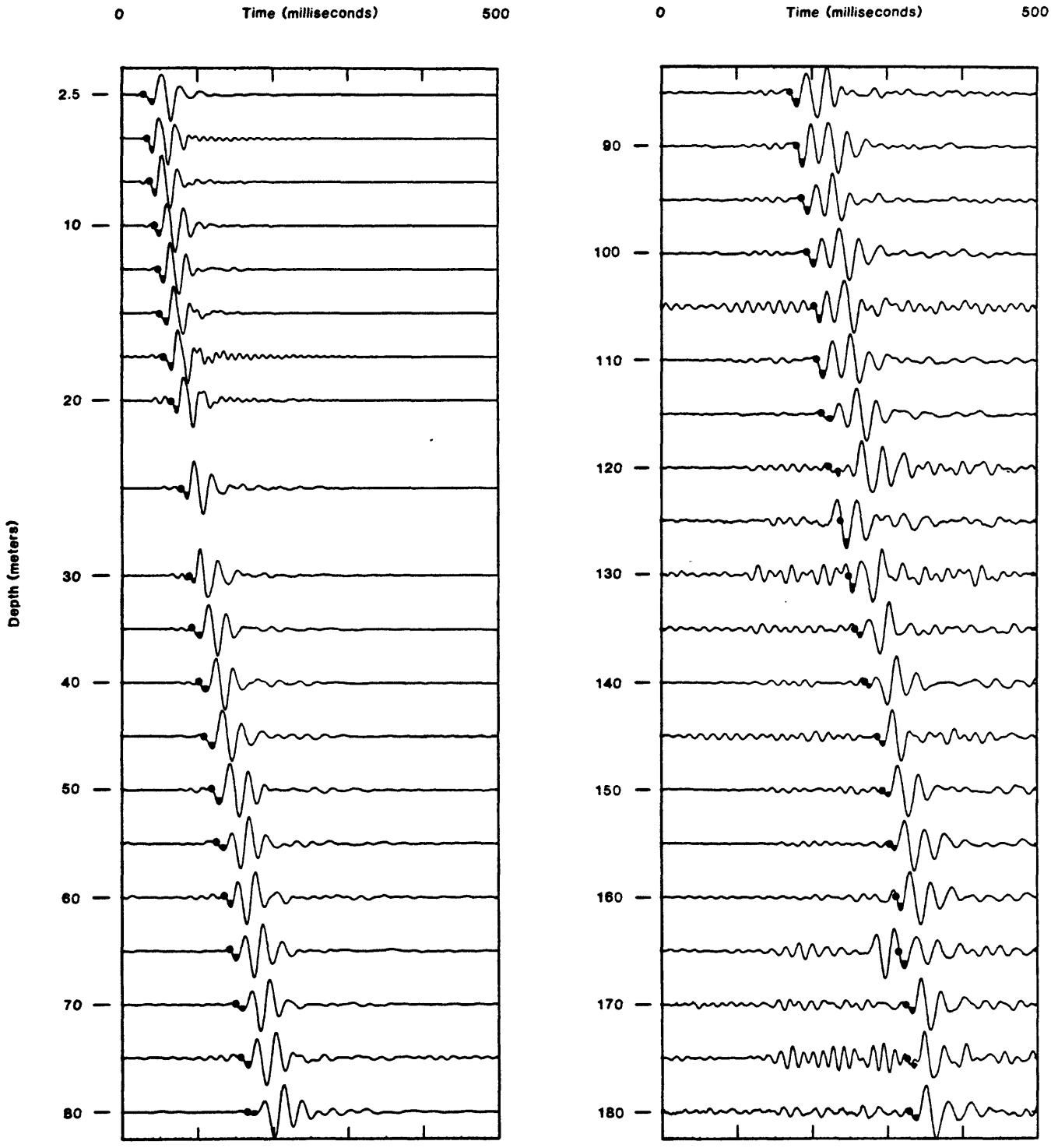

Figure 14. Red Hills record section showing S-wave picks: zero-crossings (dots) and troughs (filled).

TABLE 6

TRAVELTIMES AND AVERAGE VELOCITIES: RED HILLS BOREHOLE

Site Abbreviation: RDH
Source Offset: S-Wave = 4.0 m

Date Logged: 1-14-87
P-Wave = 4.0 m

	S-WAVE		P-WAVE	
DEPTH (M)	ZERO-CROSSING (S)	AVE VEL (M/S)	FIRST BREAK (S)	AVE VEL (M/S)
2.5	0.016	151	0.007	347
5.0	0.025	199	0.011	471
7.5	0.033	230	0.014	545
10.0	0.040	251	0.015	649
12.5	0.045	280	0.021	586
15.0	0.047	318	0.024	636
17.5	0.053	329	0.027	658
20.0	0.063	317	0.030	675
25.0	0.080	313	0.038	666
30.0	0.090	334	0.044	689
35.0	0.095	368	0.049	709
40.0	0.103	389	0.054	736
45.0	0.109	414	0.060	747
50.0	0.120	418	0.061	817
55.0	0.127	432	0.065	844
60.0	0.136	440	0.067	894
65.0	0.143	454	0.070	928
70.0	0.151	464	0.072	971
75.0	0.157	478	0.075	1000
80.0	0.166	483	0.078	1027
85.0	0.170	499	0.081	1052
90.0	0.176	510	0.082	1100
95.0	0.186	511	0.084	1135
100.0	0.192	521	0.087	1153
105.0	0.204	516	0.089	1185
110.0	0.205	538	0.091	1214
115.0	0.213	539	0.092	1243
120.0	—	—	0.096	1256
125.0	0.240	522	0.099	1257
130.0	0.250	521	0.102	1270
135.0	0.258	523	0.102	1319
140.0	0.272	515	0.106	1318
145.0	0.279	520	0.109	1328
150.0	0.288	522	0.112	1339
155.0	0.303	511	0.113	1371
160.0	0.313	511	0.115	1390
165.0	0.316	522	0.117	1411
170.0	0.326	522	0.120	1418
175.0	0.326	536	0.123	1424
180.0	0.332	542	0.125	1443

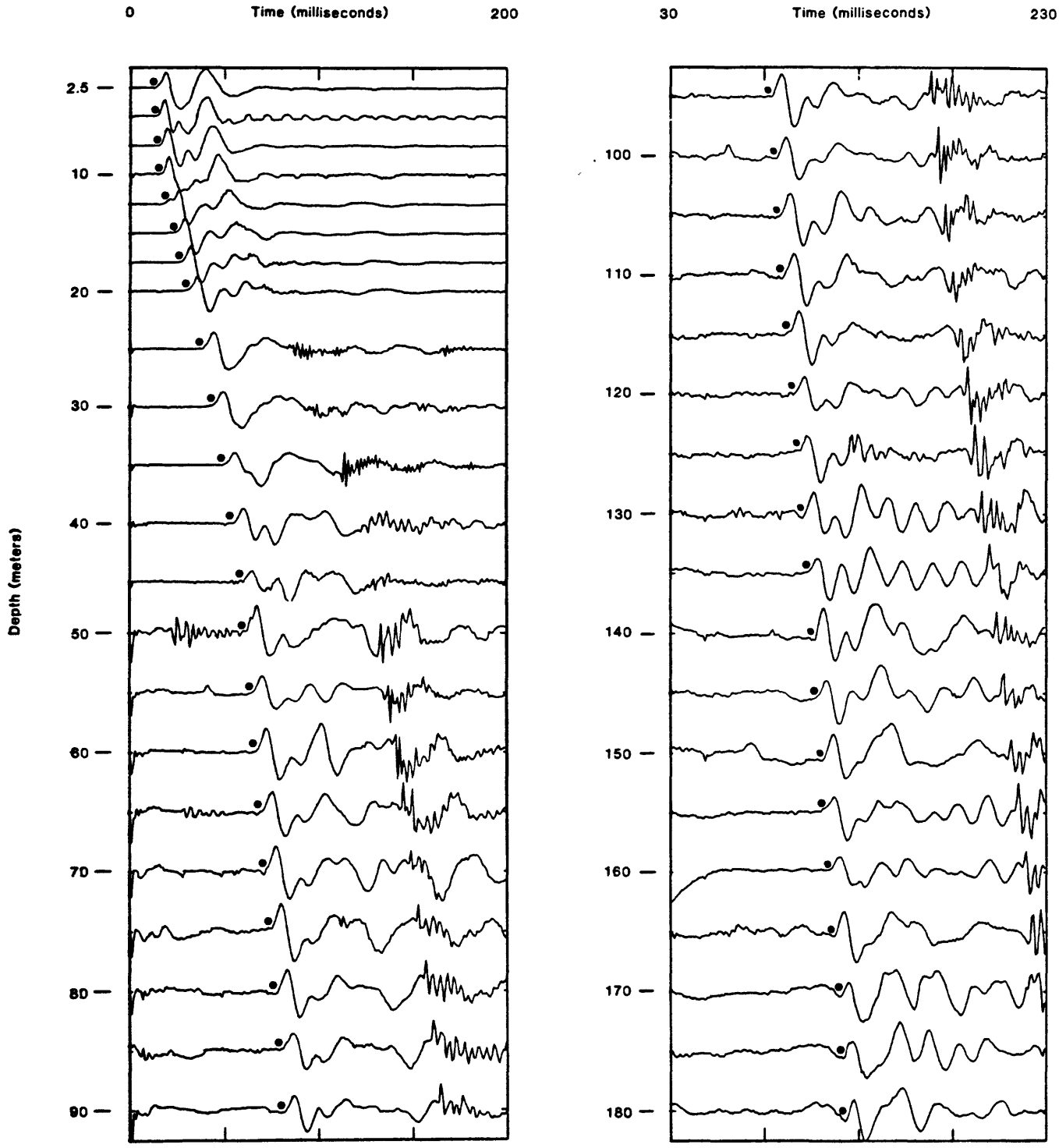

Figure 15. Red Hills record sectin showing P-wave picks.

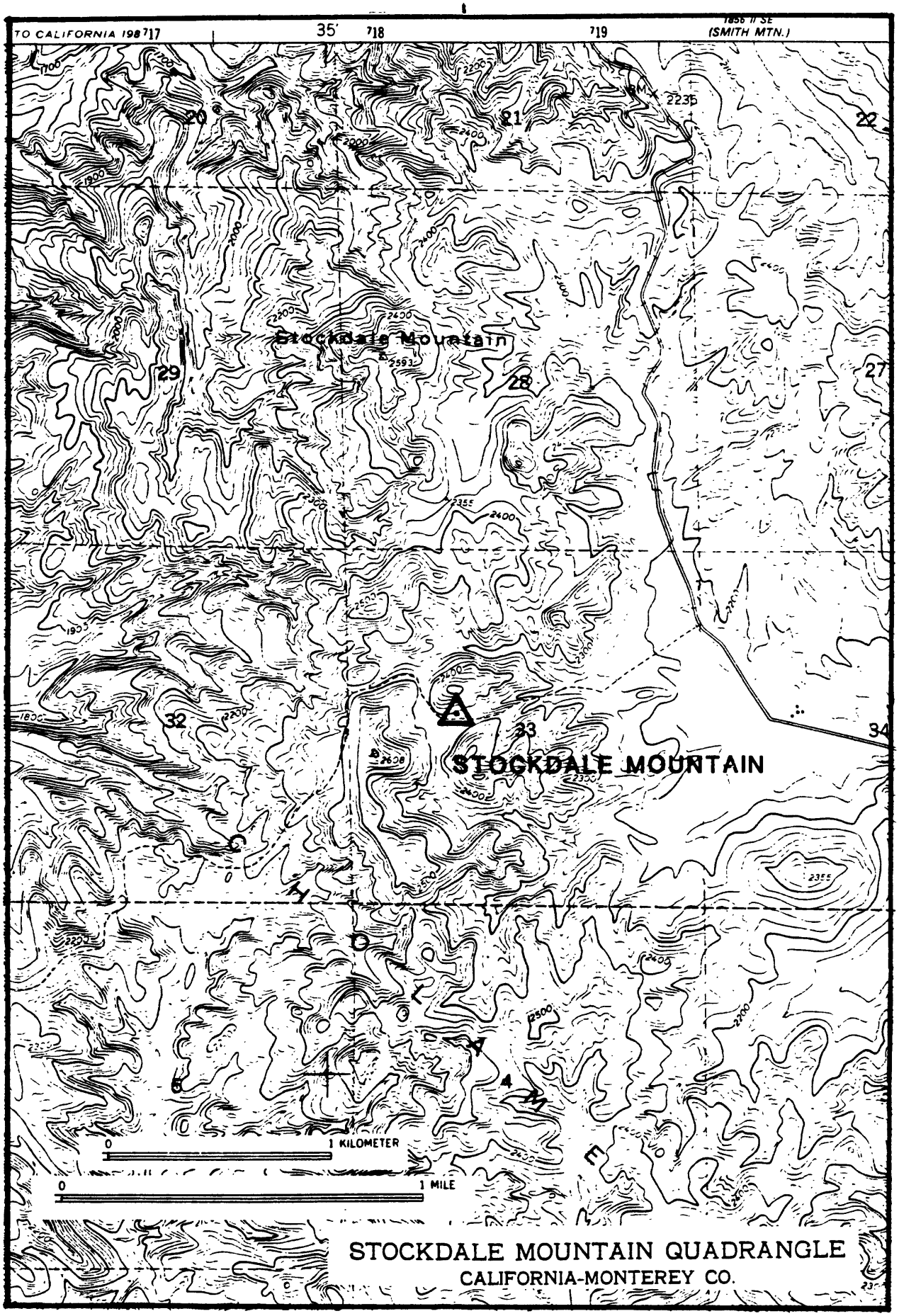

Figure 16. Location map of Stockdale Mountain borehole.

Site: STOCKDALE MOUNTAIN

Borehole completed: 7-23-86
Location: Lat. 35°58.4'N
Long. 120°34.6'W

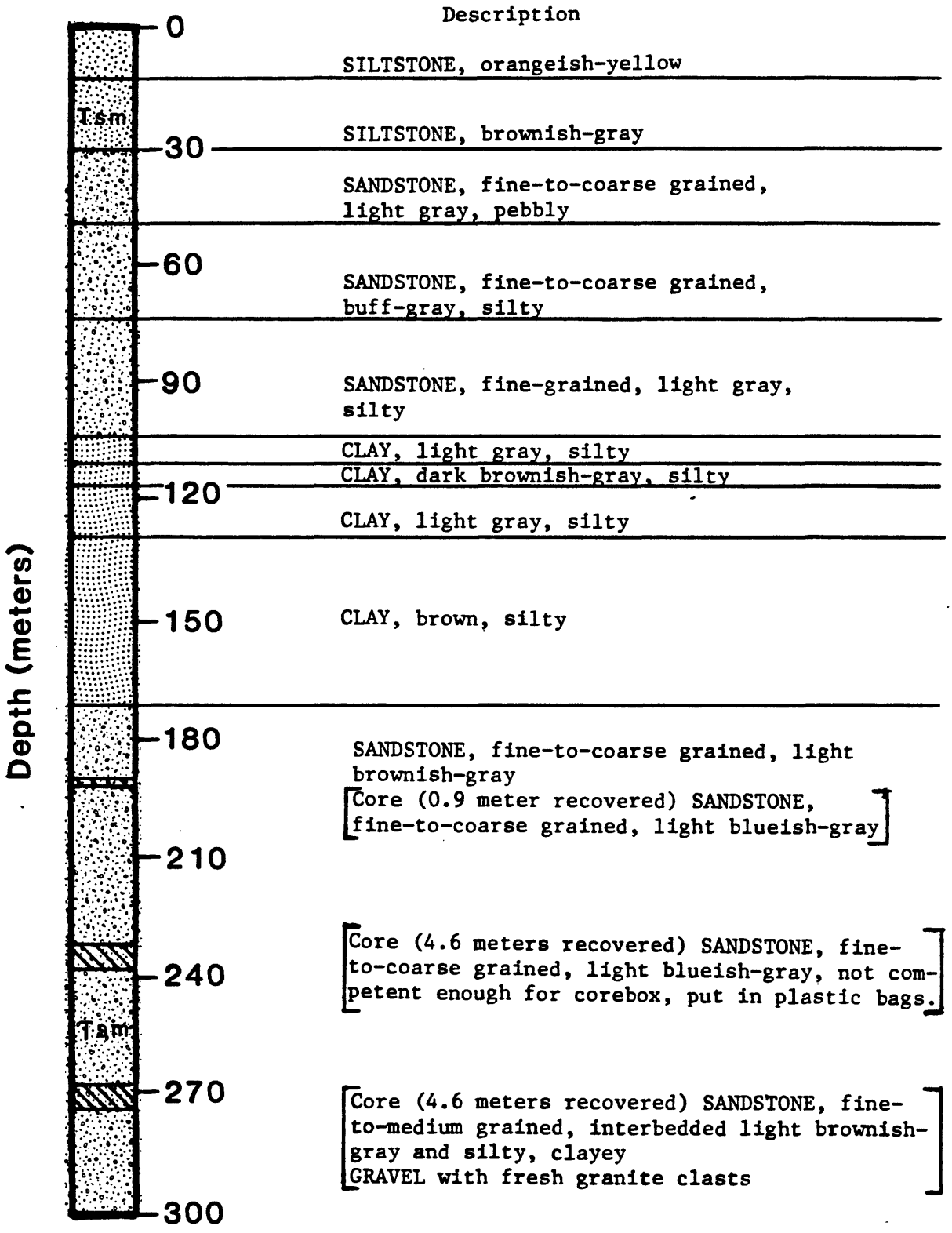

Figure 17. Geologic log of Stockdale Mountain borehole. Compiled from drill cuttings and cores. Geologic map units are from Dibblee (1974).

TABLE 7

TRAVELTIMES AND AVERAGE VELOCITIES: STOCKDALE MOUNTAIN BOREHOLE

Site Abbreviation: SDM
Source Offset: S-Wave = 4.0 m

Date Logged: 11-24-86
P-Wave = 4.0 m

	S-WAVE		P-WAVE	
DEPTH (M)	ZERO-CROSSING (S)	AVE VEL (M/S)	FIRST BREAK (S)	AVE VEL (M/S)
2.5	0.023	107	0.009	284
5.0	0.035	143	0.014	364
7.5	0.042	178	0.017	436
10.0	0.044	225	0.018	552
12.5	0.049	254	0.021	586
15.0	0.053	284	0.024	636
17.5	0.058	302	0.025	710
20.0	0.060	332	0.027	747
22.5	0.063	355	0.028	808
25.0	0.068	366	0.030	838
27.5	0.072	380	0.031	891
30.0	0.074	408	0.032	940
35.0	0.083	420	0.037	950
40.0	0.091	438	0.039	1031
45.0	0.101	446	0.045	1006
50.0	0.105	476	0.047	1072
55.0	0.114	483	0.057	974
60.0	0.122	493	0.058	1028
65.0	0.127	514	0.064	1011
70.0	0.131	533	0.066	1058
75.0	0.137	546	0.071	1055
80.0	0.144	555	0.072	1109
85.0	0.150	566	0.075	1133
90.0	0.156	578	0.078	1155
95.0	0.161	591	0.080	1189
100.0	0.168	597	0.083	1207
105.0	0.170	616	0.085	1239
110.0	0.179	614	0.087	1268
115.0	0.187	615	0.090	1283
120.0	0.194	619	0.092	1309
125.0	0.200	626	0.095	1322
130.0	0.204	638	0.098	1334
135.0	0.214	630	0.100	1345
140.0	0.222	630	0.102	1368
145.0	0.225	644	0.104	1391
150.0	0.227	660	0.106	1412
155.0	0.231	671	0.107	1445

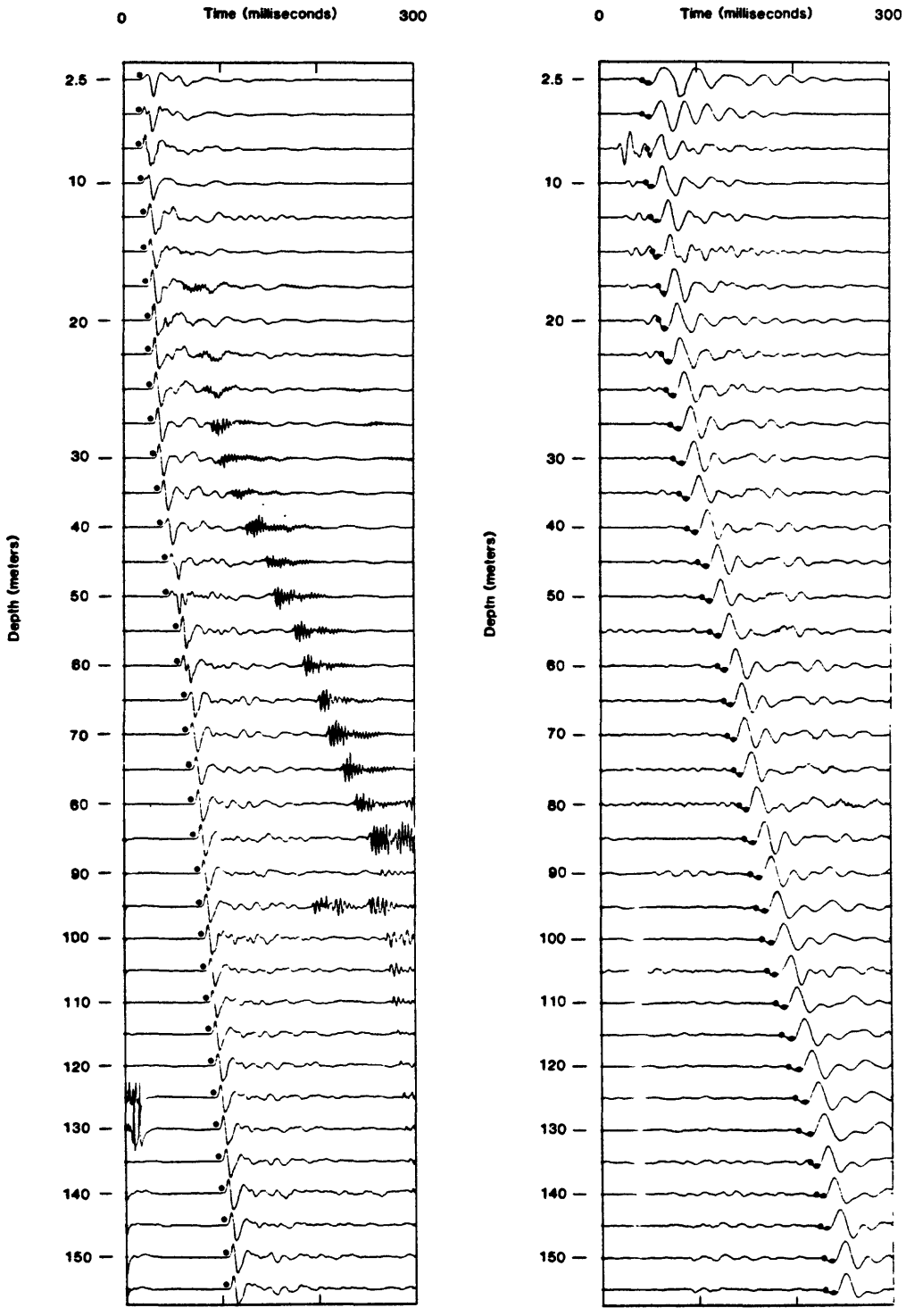

Figure 18. Stockdale Mountain record section showing P-wave (left) and S-wave picks. Two picks are shown for the S-wave: zero-crossings (dots) and troughs (filled).

Figure 19. Location map of Vineyard Canyon borehole.

Site: VINEYARD CANYON

Borehole completed: 4-2-86
Location: Lat. 35°55.3'N
Long. 120°32.0'W

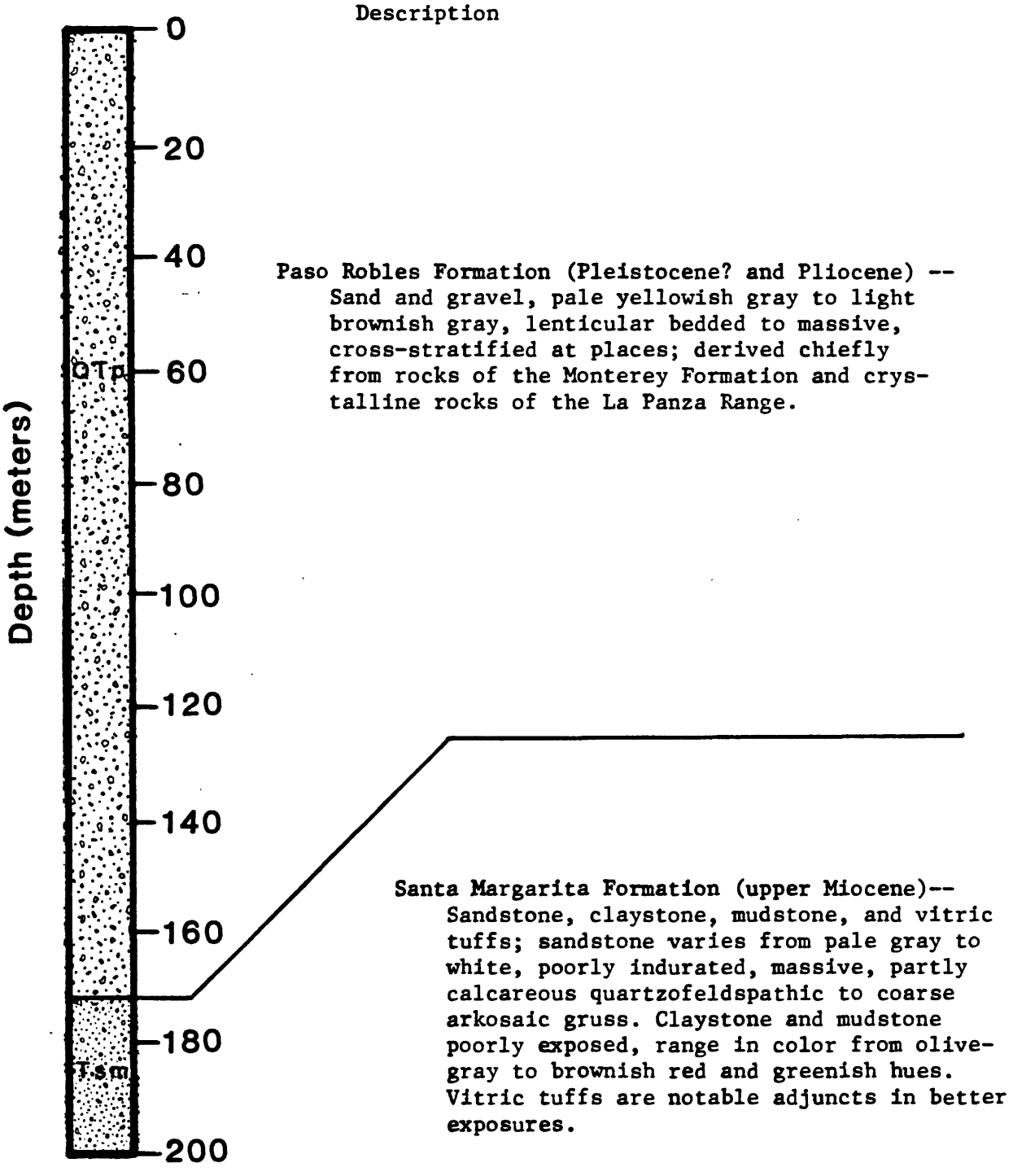

Figure 20. Geologic log of Vineyard Canyon borehole. Compiled from descriptions of geologic map units (Sims, 1989 and Dibblee, 1974).

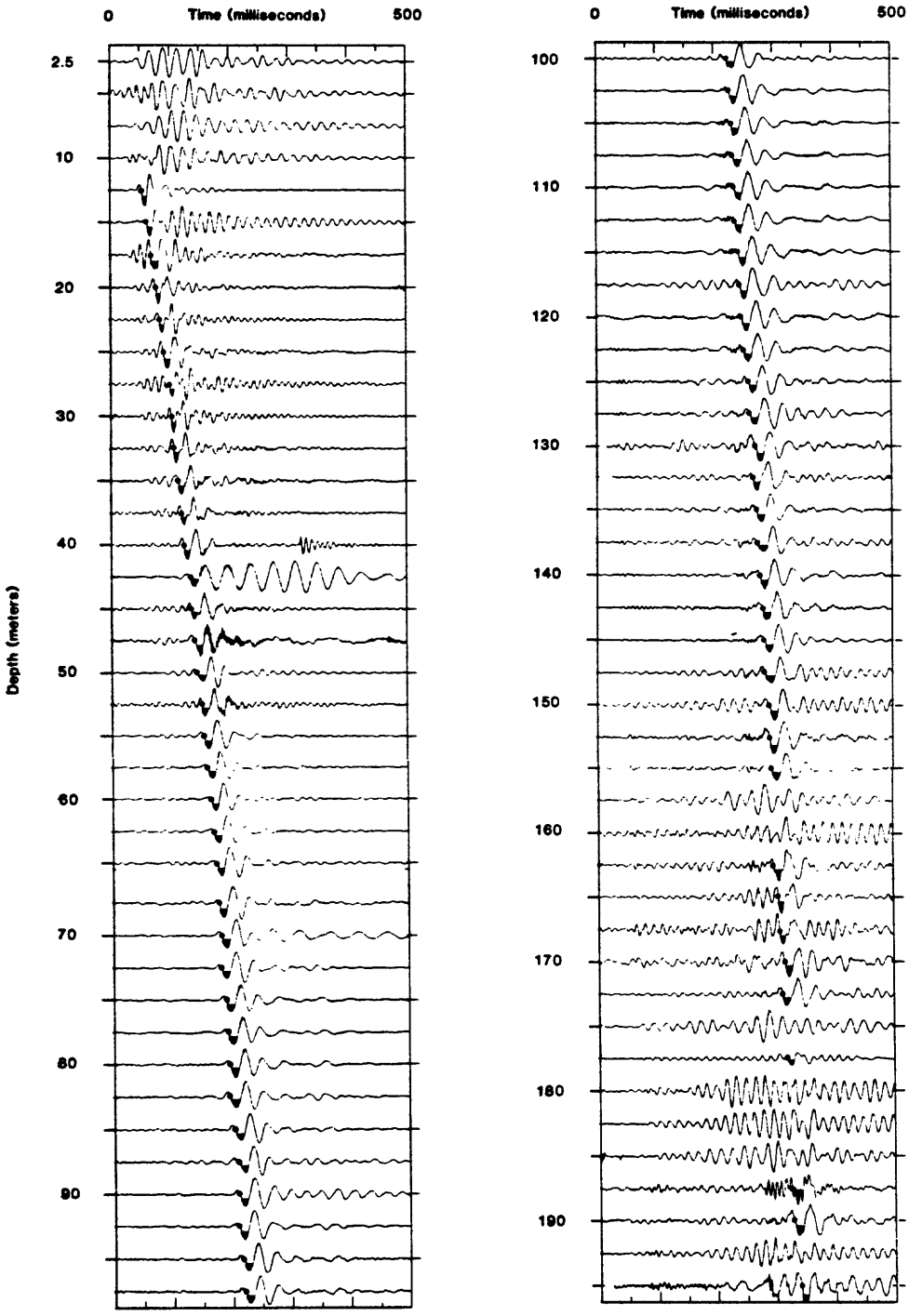

Figure 21. Vineyard Canyon record section showing S-wave picks: zero-crossings (dots) and troughs (filled).

TABLE 8

TRAVELTIMES AND AVERAGE VELOCITIES: VINEYARD CANYON BOREHOLE

Site Abbreviation: VYC — Date Logged: 6-3-86
Source Offset: S-Wave = 4.0 m — P-Wave = 2.85 m

	S-WAVE		P-WAVE	
DEPTH (M)	ZERO-CROSSING (S)	AVE VEL (M/S)	FIRST BREAK (S)	AVE VEL (M/S)
2.5	—	—	0.008	325
5.0	—	—	0.009	538
7.5	—	—	0.010	750
10.0	—	—	0.010	971
12.5	0.051	245	0.011	1096
15.0	0.060	249	0.020	746
17.5	0.068	256	0.023	758
20.0	0.076	265	0.024	826
22.5	0.083	272	0.027	830
25.0	0.089	282	0.031	806
27.5	0.098	282	0.034	811
30.0	0.102	296	0.038	794
32.5	0.106	308	0.039	835
35.0	0.112	311	0.044	799
37.5	0.117	320	0.047	803
40.0	0.121	330	0.049	823
42.5	0.132	322	0.051	840
45.0	0.135	333	0.054	841
47.5	0.140	340	0.056	841
50.0	0.147	341	0.058	856
52.5	0.150	350	0.059	884
55.0	0.154	358	0.060	911
57.5	0.160	358	0.060	952
60.0	0.164	365	0.061	979
62.5	0.170	367	0.062	1003
65.0	0.173	375	0.064	1011
67.5	0.178	379	0.066	1020
70.0	0.183	383	0.067	1042
72.5	0.183	396	0.069	1049
75.0	0.189	397	0.071	1055
77.5	0.193	402	0.073	1060
80.0	0.196	409	0.074	1080
82.5	0.196	421	0.077	1071
85.0	0.203	420	0.081	1051
87.5	0.208	422	0.084	1044
90.0	0.210	428	0.083	1086
92.5	0.208	444	0.085	1091
95.0	0.217	437	0.090	1059
97.5	0.220	443	0.092	1063
100.0	0.223	448	0.093	1080
102.5	0.226	454	0.093	1107
105.0	0.229	459	0.094	1122

TABLE 8 (continued)

TRAVELTIMES AND AVERAGE VELOCITIES: VINEYARD CANYON BOREHOLE

DEPTH (M)	S-WAVE ZERO-CROSSING (S)	S-WAVE AVE VEL (M/S)	P-WAVE FIRST BREAK (S)	P-WAVE AVE VEL (M/S)
107.5	0.235	458	0.096	1114
110.0	0.237	465	0.098	1128
112.5	0.238	473	0.098	1154
115.0	0.245	470	0.100	1156
117.5	0.245	480	0.102	1147
120.0	0.251	477	0.104	1151
122.5	0.254	482	0.106	1152
125.0	0.255	489	0.111	1124
127.5	0.263	484	0.107	1188
130.0	0.268	485	0.115	1129
132.5	0.266	498	0.116	1142
135.0	0.274	493	—	—
137.5	0.277	497	—	—
140.0	0.280	501	0.119	1177
142.5	0.279	511	—	—
145.0	0.283	513	0.118	1229
147.5	0.286	516	0.122	1210
150.0	0.295	508	0.123	1221
152.5	0.293	520	0.126	1212
155.0	0.294	526	0.128	1214
157.5	—	—	0.129	1224
160.0	—	—	0.132	1216
162.5	0.299	543	0.135	1207
165.0	0.305	541	0.132	1254
167.5	0.308	544	0.136	1236
170.0	0.317	537	0.136	1245
172.5	0.313	551	0.138	1245
175.0	—	—	0.141	1238
177.5	0.319	557	0.142	1246
180.0	—	—	0.140	1282
182.5	—	—	0.139	1309
185.0	—	—	0.140	1318
187.5	0.326	576	0.141	1326
190.0	0.331	573	0.142	1334
192.5	—	—	0.143	1343
195.0	—	—	0.148	1316